Thermal Diffusivity of $La_{1-x}Sr_xMnO_3$ ($x \leq 0.3$)[1]

A. Salazar[2,4], A. Oleaga[2] and D. Prabhakaran[3]

[1] Paper presented at the Fifteenth Symposium on Thermophysical Properties, June 22-27. 2003, Boulder, Colorado, U.S.A.

[2] Departamento de Física Aplicada I, Escuela Superior de Ingenieros, Universidad del País Vasco, Alameda Urquijo s/n, 48013 Bilbao, Spain.

[3] Clarendon Laboratory, Department of Physics, University of Oxford, Oxford, OX1 3PU, UK.

[4] Corresponding autor. Electronic mail: wupsahea@bi.ehu.es

Perovskite manganites are interesting because of their colossal magnetoresistance. In this work we present high resolution thermal diffusivity measurements of $La_{1-x}Sr_xMnO_3$ ($0 \leq x \leq 0.3$) single crystals in the temperature range from 250K to 400K. A photopyroelectric device in the standard back configuration has been used. The thermal diffusivity through second order magnetic phase transitions, as well as through first and second order structural phase transitions has been measured. The critical parameters of the sample with x = 0.3 at the ferromagnetic to paramagnetic transition have been obtained. Although the sample shows a pronounce rounding near the transition temperature, an Ising-like behavior can be recognized ($\alpha = 0.12$, $A/A' = 0.80$).

1. INTRODUCTION

In the last years great attention has been paid to perovskite manganites $L_{1-x}A_xMnO_3$ (L = lanthanide, A = alkaline earth) due to their colossal magnetoresistance, i.e. the large decrease of the electrical resistivity near the Curie temperature by applying a magnetic field [1,2]. This effect is interesting for both basic research and potential technological applications, such as magnetic recording, actuators and sensors. However, while many works have been devoted to the study of their magnetic and electrical properties, only few papers deal with their thermal transport properties.

In this work we present high resolution thermal diffusivity measurements on a set of $La_{1-x}Sr_xMnO_3$ ($0 \le x \le 0.3$) single crystals using a photopyroelectric (PPE) device in the back configuration, where an opaque slab is periodically illuminated on one side, while the other side is in contact with the pyroelectric detector [3]. This technique is specially suited to the study of the through-thickness thermal properties around phase transitions, since small temperature gradients in the sample produce a good enough signal-to-noise ratio. Therefore, the thermal parameters close to the phase transition are measured with high accuracy [4,5].

$La_{1-x}Sr_xMnO_3$ materials have a very complicated behavior, where magnetic, electronic and structural phase transitions take place [6-8]. Undoped $LaMnO_3$ is an insulator antiferromagnet with a cooperative Jahn-Teller (JT) distortion. Replacing a small amount of La^{3+} by Sr^{2+}, i.e. doping the compound with a small number of holelike charge carriers, induces drastic changes in these properties. The cooperative JT effect is suppressed, ferromagnetism develops, metallic behavior is observed and rhombohedral symmetry appears. Figure 1 shows the phase diagram for $0 \le x \le 0.35$ between 250K and 500K. As far as we are concerned there are no thermal transport measurements on these materials above room temperature.

In this work thermal diffusivity measurements from 250 K to 400 K are presented. The data reveal a dominant lattice contribution to heat conductivity. The rather low values of the thermal diffusivity, indicating a phonon mean free path of the order of the lattice spacing, correlate with local distortion of the MnO_6 octahedra. Modifications of the local structure are responsible for the anomalies at the magnetic and structural transitions. The critical behavior of the thermal diffusivity of the sample with x = 0.3 at the ferromagnetic to paramagnetic transition has been studied. Although the sample shows a high rounding near the transition temperature, an Ising-like behavior has been recognized (α = 0.12, *A/A'* = 0.80).

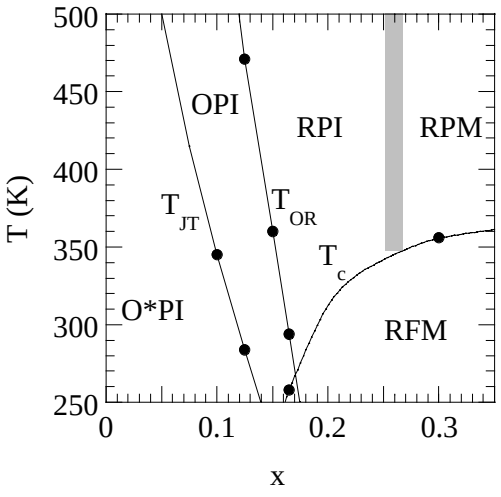

Figure 1.- Phase diagram for $La_{1-x}Sr_xMnO_3$ ($0 \le x \le 0.3$). O*: Jahn-Teller distorted orthorhombic, $c/\sqrt{2}$ < a,b; O: orthorhombic, $c/\sqrt{2} \approx$ a,b; R: rhombohedral; P: paramagnetic; F: ferromagnetic; I: insulator; M: metal; T_{JT}: Jahn-Teller transition and T_c: the Curie temperature.

2. EXPERIMENTAL PROCEDURES

Single crystals of $La_{1-x}Sr_xMnO_3$ (x = 0, 0.05, 0.10, 0.125, 0.15, 0.165 and 0.30) were grown by the floating-zone technique. The polycrystalline seeds were prepared from a stoichiometric mixture of La_2O_3, $SrCO_3$ and Mn_2O_3 calcined and sintered at 1200ºC for 72 h. Crystals were grown in an Ar-rich atmosphere at a pressure of 6-8 atm. in order to reduce manganese evaporation. The nature of the crystal surface was checked by optical and scanning electron microscopy, while X-ray powder and Laue diffraction was used to assess the phase purity, structure and crystalline quality. Surface images of polished cross-sections of the crystals are smooth, with no evidence of micro-cracks, segregation or twin boundaries. Detailed growing procedures were reported elsewhere [9]. Slices of thickness between 0.3 and 0.4 mm were cut from the grown crystals perpendicular to the growth direction (*c*-axis) for thermal diffusivity measurements. Their lattice parameters are given in Table 1.

Table 1.- Samples parameters at room temperature.

x	*a* (nm)	*b* (nm)	*c* (nm)	$c/\sqrt{2}$	Symmetry	Space group	Density (g/cm^3)
0.00	5.522	5.730	7.673	< a,b	O*	Pbnm	6.62
0.05	5.527	5.645	7.692	< a,b	O*	Pbnm	6.62
0.10	5.548	5.586	7.742	< a,b	O*	Pbnm	6.55
0.125	5.530	5.545	7.795	≈ a,b	O	Pbnm	6.54
0.15	5.505	5.544	7.790	≈ a,b	O	Pbnm	6.53
0.165	5.499	5.544	7.784	≈ a,b	O	Pbnm	6.53
0.30	5.511	5.511	13.367	-	R	$R\bar{3}c$	6.41

Thermal diffusivity measurements have been performed by a PPE setup in the standard back configuration [3]. A mechanically modulated He-Ne laser beam of 5 mW illuminates the upper surface of the sample under study. Its rear surface is in thermal contact with a 350 μm thick $LiTaO_3$ pyroelectric detector with Ni-Cr electrodes on both faces, by using a very thin layer of high vacuum silicone grease. The PPE signal is processed by a lock-in amplifier in the current mode. Both sample and detector are placed inside a nitrogen bath cryostat that allows measurements in the temperature range from 77K to 500K, at rates that vary from 100 mK/min for measurements on a wide temperature range to 10 mK/min for high resolution runs close to the phase transitions. If the sample is opaque and thermally thick ($\ell_s > \mu$) the natural logarithm and the phase of the normalized PPE voltage at a fixed temperature, i.e., the ratio of the voltage with and without a sample, are given by [3,10]

$$\ln(V_n) = \ln\left(\frac{2\dfrac{1-R_s}{1-R_p}}{1+\dfrac{e_s}{e_p}}\right) - \frac{\ell_s}{\mu_s} \tag{1}$$

$$\Psi n = -\frac{\ell_s}{\mu_s} \tag{2}$$

where R is the optical reflection coefficient, $\mu = \sqrt{D/\pi f}$ is the thermal diffusion length, D is the thermal diffusivity and e is the thermal effusivity. Subindexes s and p stand for sample and pyroelectric detector respectively.

According to Eqs. (1) and (2), both the phase Ψ_n and the natural logarithm $\ln(V_n)$ of the PPE signal have a linear dependence on $\sqrt{f}$, with the same slope m, from which the thermal diffusivity of the sample can be measured

$$D = \frac{\ell_s^2 \pi}{m^2} \tag{3}$$

On the other hand, the temperature dependence of the thermal diffusivity can be measured as follows [10,11]. First we measure the thermal diffusivity D_{ref} at a fixed temperature T_{ref}, using the linear method explained above. Then we choose a frequency for which the sample is thermally thick. Finally we change the temperature while recording the phase of the PPE signal, first for the pyroelectric detector alone and then for the sample. If we define the phase difference as $\Delta(T) = \Psi_n(T) - \Psi_n(T_{ref})$, the temperature dependence of the thermal diffusivity is given by

$$D(T) = \left[\frac{1}{\sqrt{D_{ref}}} - \frac{\Delta(T)}{\ell_s \sqrt{\pi f}} \right]^{-2} \tag{4}$$

To calibrate our PPE setup we have measured the thermal diffusivity of Cr_2O_3 across its magnetic phase transition. Cr_2O_3 is a weakly anisotropic antiferromagnet with a Néel temperature $T_N \approx 307$ K. The sample we have used is a 5 mm diameter disk with a thickness of 0.60 mm. Several measurements have been performed at frequencies of 12 Hz and 23 Hz and at heating rates between 90 mK/min and 30 mK/min, but no significant differences have been found. The temperature dependence of the thermal diffusivity is shown in Figure 2a and agree very well with the values previously reported by Marinelli and coworkers [4]. The sharpness of the dip of D at the transition indicates the good quality of the crystal as well as the high resolution of the PPE setup. In order to extract information on the critical parameters of Cr_2O_3 the experimental data of the inverse of D has been fitted to a function which is similar to the one used for specific heat [4,12]

$$1/D = B + Ct + A|t|^{-\alpha}\left(1 + E|t|^{0.5}\right) \qquad t > 0 \tag{5a}$$

$$1/D = B + Ct + A'|t|^{-\alpha}\left(1 + E'|t|^{0.5}\right) \qquad t < 0 \tag{5b}$$

where $t = \frac{T - T_N}{T_N}$ is the reduced temperature. As the thermal diffusivity is related to the specific heat c_p through the relation

$$D = \frac{K}{\rho c_p}, \tag{6}$$

where K is the thermal conductivity and ρ is the density, the inverse of the thermal diffusivity has the same critical behavior as the specific heat, provided that the thermal conductivity does not change significantly, as is the case of Cr_2O_3. Moreover, fitting $1/D$ instead of D itself is more appropriate because in the fit of D the critical exponent α is always negative since the thermal diffusivity cannot diverge at T_N. On the contrary, the inverse of D has not any

restriction in the sign of α. Accordingly, distinction between Heisenberg-like behavior (α = -0.115, *A/A'* = 1.521) and Ising-like behavior (α = 0.11, *A/A'* = 0.524) can be performed in an easy way. The temperature dependence of 1/*D* close to the magnetic phase transition of Cr_2O_3 is shown in Figure 2b. The two branches have been simultaneously fitted to Eqs. (5). The parameters of the best fitting are α = -0.039, *A/A'* = 1.27 in perfect agreement with the result reported in Ref. [4] for the specific heat in the same temperature range, indicating a no universal behavior of this material.

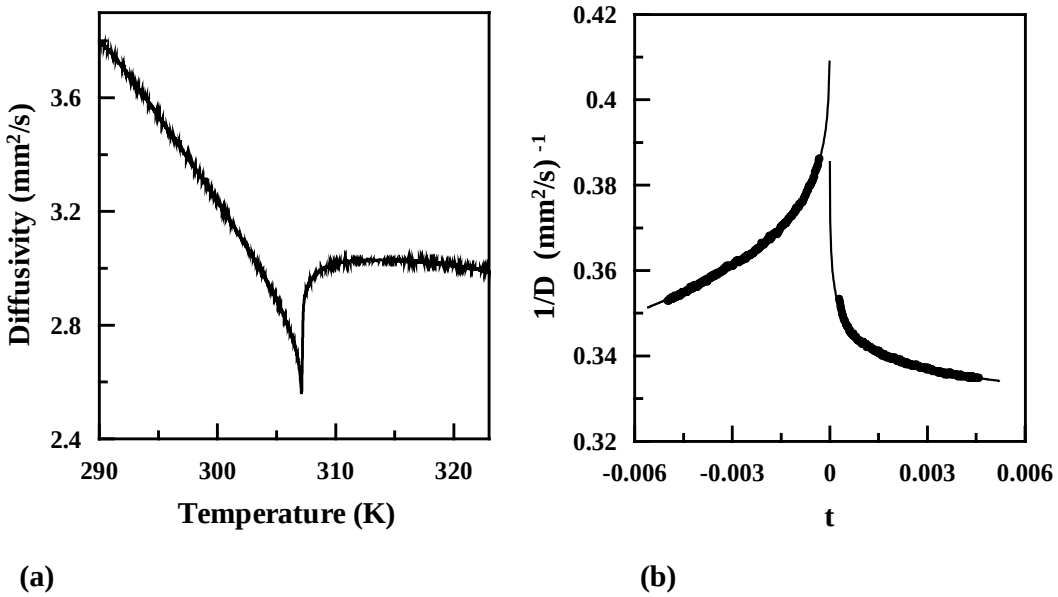

Figure 2.- (a) Temperature dependence of the thermal diffusivity of Cr_2O_3 around the antiferromagnetic to paramagnetic phase transition. (b) Inverse of the thermal diffusivity versus the reduced temperature. The solid line corresponds to the best fit to Eqs. (5).

3. EXPERIMENTAL RESULTS AND DISCUSSION

The temperature dependence of the thermal diffusivity along the *c*-axis of the seven $La_{1-x}Sr_xMnO_3$ crystals are shown in Figure 3. All of the *D* values are quite low for crystalline solids, with the data for lightly doped samples (x = 0.1-0.17) near room temperature falling in the typical range of glasses (*D* = 0.4-0.8 mm^2/s). Moreover, from the values of the specific heat and density the room temperature thermal conductivity can be calculated using Eq. (6). Its values are shown in Table 2, and lie in the typical range of amorphous materials (0.5-5 $Wm^{-1}K^{-1}$). On the other hand, from the values of the electrical resistivity *r* [13] the upper limit of the electronic contribution to the total thermal conductivity can be calculated using the Wiedemann-Franz law ($K_e = L_oT/r$; where $L_o = 2.45\times10^{-8}$ $W\Omega/T^2$ is the Lorentz number). Its values are also shown in Table 2. As can be seen the electronic contribution to the thermal conductivity is negligible even for the sample with x = 0.3, that exhibits a metallic behavior. Therefore the heat conduction in these materials is due to phonons.

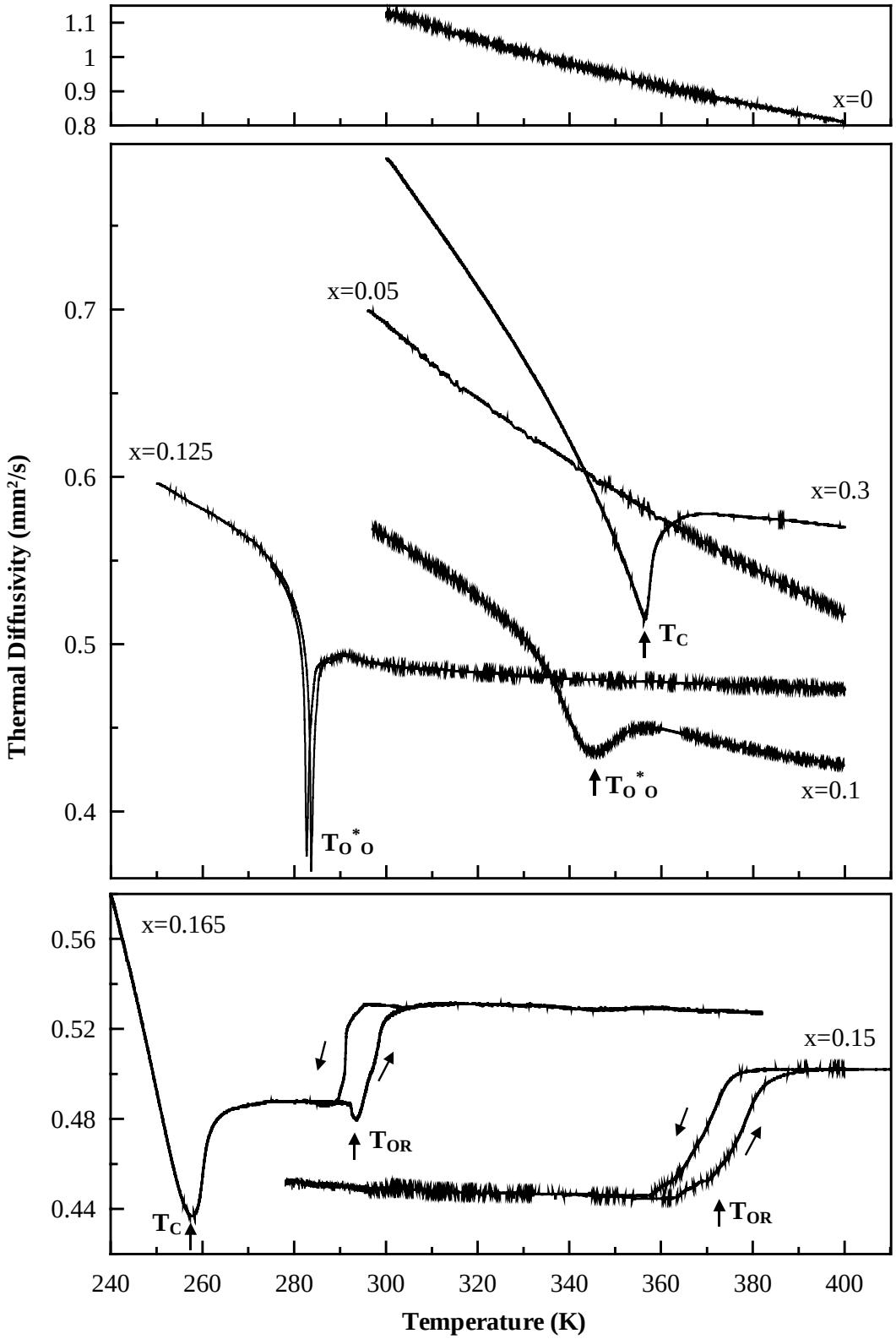

Figure 3.- Thermal diffusivity versus temperature for $La_{1-x}Sr_xMnO_3$ single crystals.

Table 2.- Thermal parameters at room temperature.

x	D (mm^2/s)	c_p* ($Jkg^{-1}K^{-1}$)	K ($Wm^{-1}K^{-1}$)	Resistivity* (Ωm)	K_e ($Wm^{-1}K^{-1}$)
0.00	1.15	578	4.4	2×10^{2}	3×10^{-8}
0.05	0.77	600	3.1	10	10^{-7}
0.10	0.56	620	2.3	10^{-2}	7×10^{-4}
0.125	0.47	594	1.8	2×10^{-3}	4×10^{-3}
0.15	0.45	620	1.8	8×10^{-4}	0.01
0.165	0.52	608	2.1	8×10^{-4}	0.01
0.30	0.90	575	3.3	6×10^{-5}	0.12

*From Ref. [13].

The kinetic theory provides the simplest model to express the thermal conductivity of a dilute gas $K = \rho c_p \bar{v} \lambda / 3$, where $\bar{v}$ is the mean speed of the carriers and λ is their mean free path between collisions. This result has been extensively used to determine the mean free path in non-metallic materials where heat is carried entirely by phonons, as is the case of our samples. Substituting this expression into Eq. (6) an interpretation of the thermal diffusivity in terms of the scattering properties of the heat carriers is obtained

$$D = \frac{1}{3} \bar{v} \lambda \tag{7}$$

Since at room temperature $\bar{v} \approx 3500$ m/s [14], the phonon mean free path for the undoped sample is about 10 Å. As the Sr concentration increases λ is reduced, reaching the minimum value of 4 Å at x = 0.15, that is of the order of the distance between the Mn atoms. Higher Sr concentration produces an increase of λ up to 8 Å at x = 0.3.

The thermal diffusivity far away from phase transitions decreases upon warming up the sample (see Figure 3). This is due to the fact that in an insulator λ is limited by the phonon-phonon scattering and should be a decreasing function of T or approach a constant value because of saturation at high temperatures.

The singularities of Figure 3 correspond to the three kinds of phase transitions that these materials undergo in the temperature range of this study (see Figure 1). Regarding the magnetic transition the samples with x = 0.165 and x = 0.30 experience a ferromagnetic to paramagnetic transition at T_c that is characterized by a dip in the thermal diffusivity. As in the case of the Cr_2O_3 sample the experimental data of $1/D$ of $La_{0.7}Sr_{0.3}MnO_3$ have been fitted to Eqs. (5). The results are shown in Figure 4 and an Ising-like behavior can be recognized (α = 0.12±0.01, A/A' = 0.80±0.15).

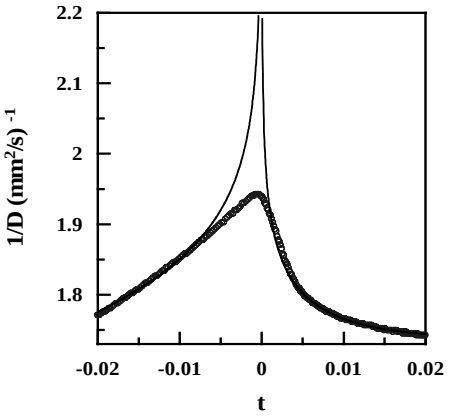

Figure 4.- Inverse of the thermal diffusivity of $La_{0.7}Sr_{0.3}MnO_3$ versus the reduced temperature. The solid line corresponds to the best fit to Eqs. (5).

However, as the dip is not as sharp as in the case of Cr_2O_3 and shows a pronounced rounding near the transition temperature, many points close to T_c have been suppressed in the fitting, reducing the reliability of the result, that has to be considered as a first approach. Actually rounding poses a severe constraint on the analysis of asymptotic behavior. This is due to the fact that thermal transport measurements strongly depend on the internal structure of the material and only extremely perfect single crystals can be used for investigation of critical behavior. In the case of the sample with x = 0.165 the rounding is so emphasized that the critical parameters cannot be obtained.

The structural transition between the Jahn-Teller distorted orthorhombic phase and the octahedron rotated orthorhombic phase (O*O) at T_{JT} shows a broad shallow minimum without hysteresis for the sample with x = 0.10, indicating its second order nature; but there is a narrow and abrupt dip with a 1 K hysteresis in the sample with x = 0.125, showing its first order nature. This change of the O*O transition from second order to first order as T_{JT} approaches T_c has already been reported [13].

On the contrary, the structural transition from orthorhombic to rhombohedral (OR) at T_{OR} in the samples with x = 0.15 and 0.165 is characterized by a step with a 5-8% higher *D* at the rhombohedral phase. The 8 K hysteresis indicates the first order nature of this transition. In the rhombohedral symmetry *D* remains constant over a wide range of temperature.

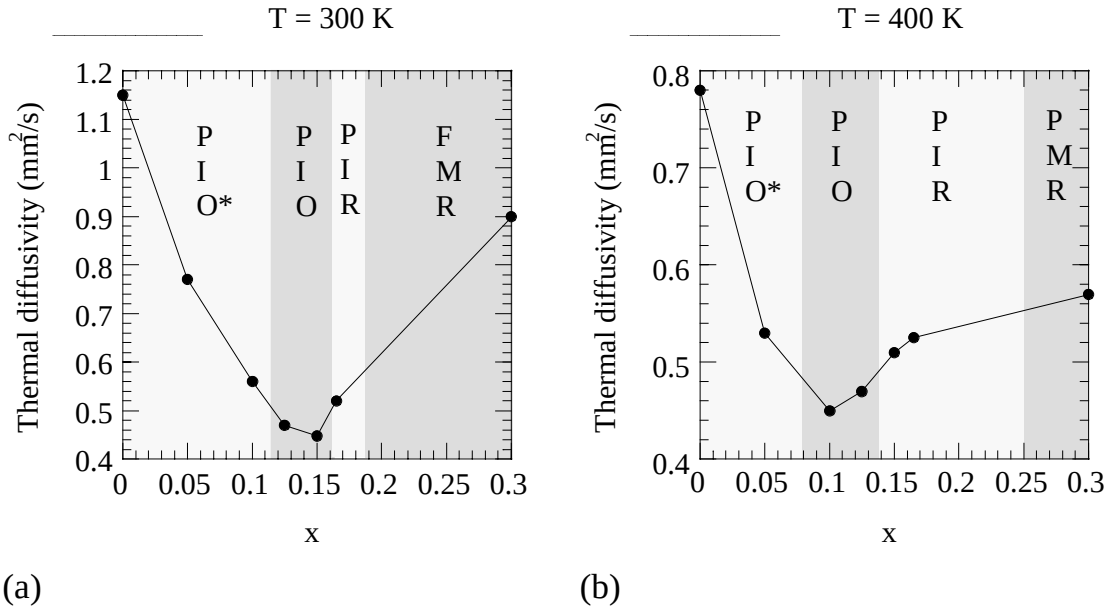

Figure 5.- Thermal diffusivity against Sr concentration at two temperatures: (a) T = 300 K and (b) T = 400 K. The continuous line is a guide for the eye.

Figure 5 shows the evolution of the thermal diffusivity with the Sr concentration at room temperature and at 400 K. In both cases a drastic reduction of the phonon mean free path is observed for x between 0.1 and 0.17. Then the thermal diffusivity increases as the Sr concentration does, but without reaching the value of the undoped sample. A similar behavior for the thermal conductivity at 50 K has already been reported [15]. There, the reduction of the thermal conductivity was ascribed to the crossover from localized to itinerant electrons associated to the insulator to metal transition. However, in the room temperature results of Figure 5a three phase transitions (O→R, P→F, I→M) take place in a short x range and

therefore it is difficult to explain the reason of this rise in diffusivity. In order to overcome this limitation, measurements at 400 K are shown in Figure 5b. At this temperature there are only two phase transitions (O→R, I→M) which, besides, are more separated. The results suggest that the rise in diffusivity as the Sr concentration increases is related to the structural change from the orthorhombic to the rhombohedral phase. This is also supported by the fact that in the samples where there is an O→R transition, x = 0.15 and 0.165, there is a step-like rise in diffusivity as the temperature increases (see Figure 3).

REFERENCES

1. M.B. Salamon and M. Jaime, *Rev. Mod. Phys.* **73**:583 (2001).
2. E. Dagotto, T. Hotta and A. Moreo, *Phys. Rep.* **344**:1 (2001).
3. M. Chirtoc, D. Dadarlat, D. Bicanic, J.S. Antoniow and M. Egée, in Progress in Photothermal and Photoacoustic Science and Technology, A. Mandelis ans P. Hess, ed. (SPIE, Bellingham, Washington, 1997), Vol. 3.
4. M. Marinelli, F. Mercuri, U. Zammit, R. Pizzoferrato, F. Scudieri and D. Dadarlat, *Phys. Rev. B* **49**:9523 (1994).
5. J. Thoen and C. Glorieux, *Thermochimica Acta* **304/305**:137 (1997).
6. Y. Moritomo, A. Asamitsu and Y. Tokura, *Phys. Rev. B* **56**:12190 (1997).
7. G.-L. Liu, J.-S. Khou and J.B. Goodenough, *Phys. Rev. B* **64**:144414 (2001).
8. J. Hemberger, A. Krimmel, T. Kurz, H.-A. Krug von Nidda, V. Yu. Ivanov, A.A. Mukhin, A.M. Balbashov and A. Loidl, *Phys. Rev. B* **66**:094410 (2002).
9. D. Prabhakaran, A.I. Coldea, A.T. Boothroyd and S.J. Blundell, *J. Crystal Growth* **237-239**: 806 (2002).
10. A. Salazar, *Rev. Sci. Instrum.* **74**:825 (2003).
11. S. Delenclos, M. Chirtoc, A. Hadj Sahraoui, C. Kolinsky and J.M. Buisine, *Rev. Sci. Instrum.* **73**:2773 (2002).
12. A. Kornblit and G. Ahlers, *Phys. Rev. B* **11**:2678 (1975).
13. G.-L. Liu, J.S. Zhou and J.B. Goodenough, *Phys. Rev. B* **64**:144414 (2001).
14. Kh.G. Bogdanova, A.R. Bulatov, V.A. Golenishchev-Kutuzov, L.V. Elokhina, A.V. Kapralov, A.V. Korolev, E.A. Neifel'd and M.M. Shakirzyanov, *Physics of the Solid State* **45**:298 (2003).
15. J.S. Zhou and J.B. Goodenough, *Phys. Rev. B* **64**:024421 (2001).